A Beam-Steering Reconfigurable Antenna for WLAN Applications

Zhouyuan Li, Elsayed Ahmed, Ahmed M. Eltawil, *Senior Member, IEEE*, and Bedri A. Cetiner, *Member, IEEE*

Abstract—A multifunctional reconfigurable antenna (MRA) capable of operating in nine modes corresponding to nine steerable beam directions in the semisphere space $\{-30°, 0°, 30°\}; \phi \in \{0°, 45°, 90°, 135°\}$) is presented. The MRA consists of an aperture-coupled driven patch antenna with a parasitic layer placed above it. The surface of the parasitic layer has a grid of 3×3 electrically-small square-shaped metallic pixels. The adjacent pixels are connected by PIN diode switches with ON/OFF status to change the geometry of the parasitic surface, which in turn changes the current distribution on the antenna, thus provides reconfigurability in beam steering direction. The MRA operates in the IEEE 802.11 frequency band (2.4—2.5 GHz) in each mode of operation. The antenna has been fabricated and measured. The measured and simulated impedance and radiation pattern results agree well indicating an average of ~ 6.5 dB realized gain in all modes of operation. System level experimental performance evaluations have also been performed, where an MRA equipped WLAN platform was tested and characterized in typical indoor environments. The results confirm that the MRA equipped WLAN systems could achieve an average of 6 dB Signal to Noise Ratio (SNR) gain compared to legacy omni-directional antenna equipped systems with minimal training overhead.

Index Terms—Beam-steering, reconfigurable antenna, full-wave analysis, signal to noise ratio.

I. INTRODUCTION

WIRELESS communication technology has grown rapidly in recent years. The IEEE 802.11 b/g standards operating in the 2.4 GHz band have been widely accepted and used in numerous wireless products such as routers, cell phones and laptops. However, for such systems to achieve the desired high data rate performance, relatively large Signal to Noise ratios (SNR) is required since some other electronic devices such as Bluetooth and microwave oven also operate in the 2.4 GHz band and present noise.

In this paper, a multifunctional reconfigurable antenna (MRA) is presented to provide improved performance in

wireless systems. MRAs have gained a significant interest to achieve dynamically changeable antenna properties in frequency, radiation pattern and polarization, by modifying its architecture [1]–[6]. The performance improvements of multiple-input multiple-output (MIMO) systems equipped with reconfigurable antennas have extensively been studied in the literature [7]–[11]. In [7]–[10], reconfigurable dipole, leaky-wave, and spiral antennas were used as antenna elements in MIMO systems, and capacity improvement of these systems was confirmed. The reconfigurability of these antennas was achieved by integrating switches or varactors directly into the driven antenna. This integration approach is disadvantageous due to the conflicting design requirements of the driven antenna and the switching network (individual switches and control circuitry). In [11], a reconfigurable antenna that can steer its beam into three directions was proposed, where the switching network is separated from the driven antenna, but they are both located on the same layer. The reconfigurable antenna of this work, which is capable of steering its beam into nine directions, relies on a parasitic layer technique, where the driven antenna and the switching network are placed on different layers, thereby completely separated. This approach enables individually optimizing the designs of the driven antenna and the switching network, thereby providing enhanced reconfigurability. The presented MRA steers its beam into nine different directions corresponding to nine modes of operation by configuring the surface geometry of the parasitic layer, where 3×3 electrically small square-shaped metallic pixels (*parasitic pixel surface*) are connected by PIN diode switches with ON/OFF status. The nine beam steering directions are ($\theta \in \{-30°, 0°, 30°\}; \quad \phi \in \{0°, 45°, 90°, 135°\}$) operating in 802.11 b/g band. The PIN diode switches integrated in the proposed MRA are on the *parasitic pixel surface* of the parasitic layer, which is separated from the driven antenna layer. With the beam steering capability, leakage (interference) both from and to the node of interest can be minimized in unintended directions while the SNR can be maximized in the desired direction. Full-wave analyses by HFSS [12] and multiobjective genetic algorithm optimization [13]–[16] were jointly employed to determine the interconnecting PIN diode switches' status (i.e., ON/OFF) corresponding to the targeted nine modes of operation.

The advantages of the MRA as compared to the antenna presented in [17] can be summarized as follows: 1) the beam steering capability is enhanced. The presented MRA can perform beam steering in nine directions in the semisphere space ($\theta \in \{-30°, 0°, 30°\}; \phi \in \{0°, 45°, 90°, 135°\}$) instead of only five directions ($\theta \in \{-30°, 0°, 30°\}; \phi \in \{0°, 90°\}$) in [17].

2) The parasitic surface only consists of 3×3 metallic square pixels instead of 4×4 metallic rectangular pixels, thus the complexity of the MRA is reduced. 3) Real PIN diode switches along with a sophisticated biasing circuitry have been used instead of ideal perfect open/short connection, thus providing insight in the practical limitations of the antenna.

The impedance and radiation characteristics of the fabricated individual MRA prototypes were measured. The measured results were compared with those of the simulations, indicating an average of ~6.5 dB realized gain over the frequency band of 2.4–2.5 GHz for all modes of operations.

The beam steering capability and associated system level gains of the MRA was also tested in an experimental system setting based on an IEEE 802.11 b/g system in a typical indoor environment. However, in this paper, instead of using reconfigurable antennas in a MIMO system [7]–[11], the proposed MRA is employed as one node of the SISO system, while the other node is a dipole antenna. Because of the enhanced beam steering capability of the MRA with 9 beam steering directions, it would be much easier and gives more understanding of the functionality of the MRA when the MRA is tested in a SISO system. The results confirm the advantages of the MRA and show that the proposed MRA equipped system achieves ~6 dB SNR gain compared to the legacy omni-directional antenna equipped system.

II. ANTENNA STRUCTURE AND WORKING MECHANISM

A. MRA Design and Component Models

Structure of the MRA: The top view photograph of the MRA is shown in Fig. 1(a). This MRA employed aperture-coupled feed mechanism for RF feeding similar to the MRA presented in [17]. The main two components of the MRA architecture are, namely, the driven patch antenna and parasitic layer as shown in Fig. 2. The driven patch (19.3×19.3 mm^2) is designed to operate at in the frequency band of 2.4–2.5 GHz and is fed by a 50-Ohm microstrip line through an aperture (21.4×1.4 mm^2) etched on the center of the common ground plane. The feed layer ($90 \times 90 \times 0.508$ mm^3) and patch layer ($90 \times 90 \times 3.048$ mm^3) are built respectively by using the substrate Rogers 4003C ($\varepsilon_r = 3.55, \tan \delta = 0.0021$) [18]. The same substrate ($98 \times 90 \times 1.524$ mm^3) is used to form the parasitic layer above the driven patch. Notice that there is a 7.62 mm gap between the parasitic layer and driven patch antenna, where the gap is filled with the RO4003C. The reconfigurable parasitic surface, which consists of 3×3 square-shaped metallic pixels connected by PIN diode switches with ON/OFF status, is formed on the top surface of the parasitic layer with individual pixel size being 15×15 mm^2. Thus the geometry of the parasitic surface can be configured by switching ON/OFF the PIN diode switches. DC bias lines are also formed on the parasitic layer but on the backside of the substrate, where the backside of the whole parasitic layer can be seen in Fig. 1(b). Vias are plated through the parasitic layer so that DC bias lines can be connected to the PIN diode switches on the parasitic surface. Four different kinds of components are used on the parasitic layer as shown in the magnified sections of Figs. 1(a) and 1(b):

1) PIN diode switches are used in between all square-shaped pixels. Metallic pixels are connected/disconnected by switching ON/OFF the PIN diode switches to change the geometry of the parasitic surface, which in turn change the current distribution, and thus antenna characteristics.

2) Inductors are placed along the DC bias lines as RF chokes. The SRF (self resonant frequency) of the RF choke is chosen to be around 2.5 GHz, thus RF chokes would appear as high impedance in 802.11 b/g band to minimize the current on the bias lines, thereby minimizing the mutual coupling effects of the bias lines on the antenna performance.

3) Inductors are also placed in between all pixels. In this manner, all the pixels can be DC grounded together to provide ground for DC biasing purpose. The SRF of these inductors was chosen to be the same value as RF chokes to keep the high RF impedance between pixels.

4) DC block capacitors are used to properly bias the PIN diode switches as shown in Fig. 1. The SRF of DC block capacitor is around 2.5 GHz to provide low RF impedance in 802.11 b/g band. In this way, the effect of DC block capacitor on RF performance is minimized.

The manufacturer details [19]–[21] of the above 4 components are shown in Table I. The equivalent circuit of the biasing scheme is explained in the following paragraph.

Equivalent Circuit Models Used in MRA: The DC biasing scheme of the PIN switch is shown in Fig. 3. It can be seen that the 4 different lumped components mentioned above are required to properly bias the PIN diode. Typically, 1 V DC power supply on the PIN diode would be sufficient to turn on the switch, while 0 V will keep the switch in OFF status.

The equivalent circuit models of these lumped components are obtained by using their scattering parameters provided by the manufacturers and are shown in Fig. 4. These equivalent circuit models are used in the design of the MRAs by full-wave HFSS analyses.

B. Working Mechanism

The working mechanism of an antenna system, which is composed of one driven antenna and multiple parasitic elements, can be described by the theory of reactively controlled directive arrays developed by R. F. Harrington [22]. It was shown that the main beam direction of the driven antenna can be directed into a desired direction by the proper reactive loading of the parasitic elements. In the presented MRA, the proper reactive loading corresponds to a specific geometry of the parasitic pixel surface, which is obtained by switching ON/OFF the PIN diode switches between adjacent pixels of this surface [23].

The presented MRA is aimed to steer its main beam in nine directions in the semisphere space ($\theta \in \{-30°, 0°, 30°\}; \phi \in \{0°, 45°, 90°, 135°\}$). Fig. 5 illustrates the planes in which the beam is steered, and the definitions of the beam-steering angles (θ and ϕ).

C. Optimization Methodology

To find the optimum switch status for each of the 9 beam steering directions, multiobjective genetic algorithm (GA) is utilized [23]. The multiobjective GA is different from
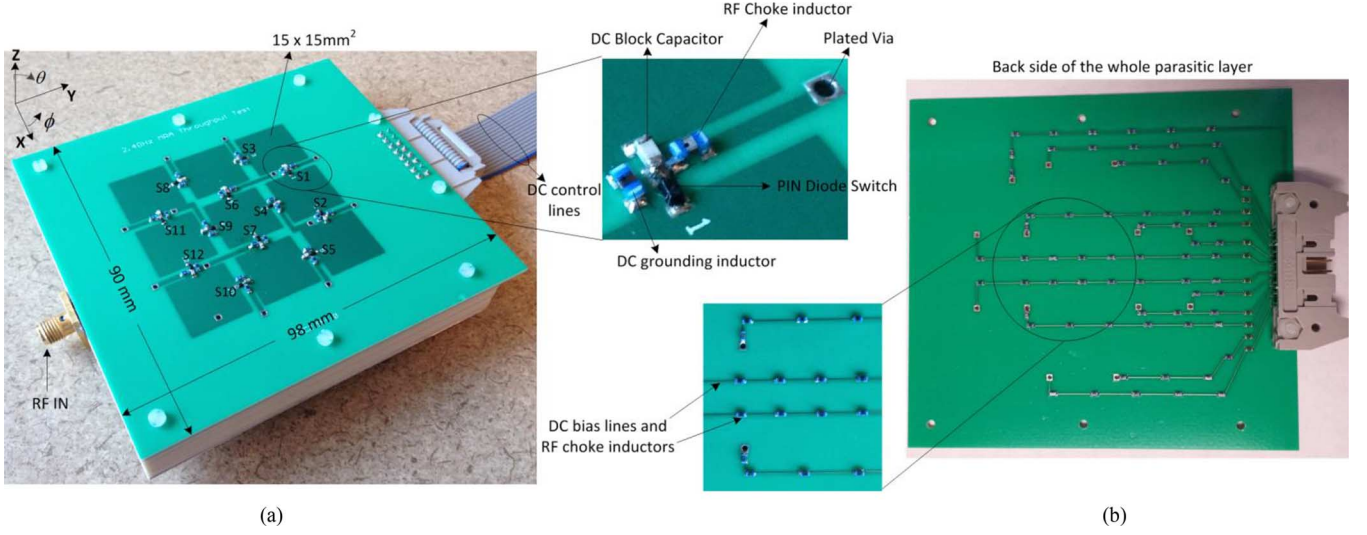
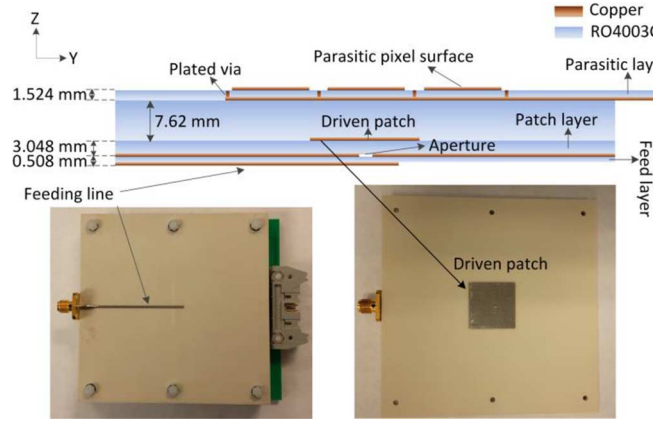Fig. 1.   (a) Top view photograph of MRA. (b) Blackside of the whole parasitic layer.

Fig. 2.   Cross Section of the MRA with top views of RF feed and driven patch.

TABLE I
LUMPED COMPONENTS USED IN MRA

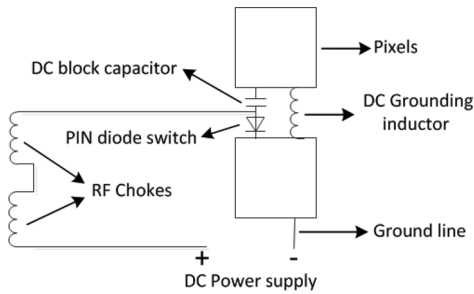| Manufacturer	Type	Value	SRF
Skyworks SMP1345	PIN diode switch	N/A	N/A
Coilcraft 0603 HP	RF choke	39 nH	2.5 GHz
Coilcraft 0603 HP	DC grounding inductor	39 nH	2.5 GHz
Murata 0603	DC block capacitor	8 pF	2.5 GHz

Fig. 3.   DC biasing scheme of the PIN diode switch.

the single-objective GA in the sense that it has more than one aim which may conflict with each other and should be evaluated simultaneously. There are 3 objectives/aims need to be satisfied, namely: a) one of the beam directions of
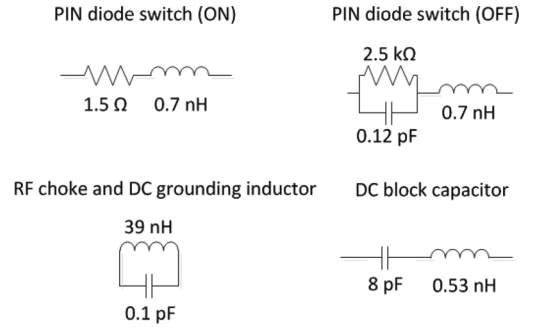

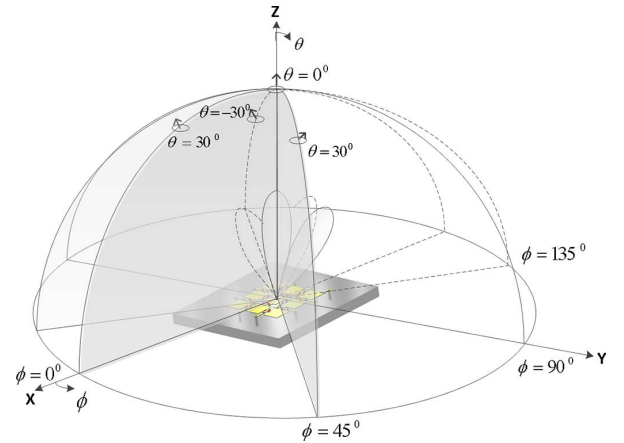Fig. 4.   Equivalent circuit models of lumped components.

Fig. 5. Beam-steering capabilities of an MRA: $\theta \in \{-30°, 0°, 30°\}$; $\phi \in \{0°, 45°, 90°, 135°\}$.

($\theta \in \{-30°, 0°, 30°\}$; $\phi \in \{0°, 45°, 90°, 135°\}$) with maximum gain above 6 dB; (b) desired frequency bandwidth (BW) of ~4% covering 2.4–2.5 GHz and (c) linear polarization with axial ratio above 10 dB in the maximum gain direction. Thus the objective functions are defined as below:

$$
\begin{aligned}
obj_1 &= \text{Gain}\,(f_0, \theta, \phi) & \text{Gain} \geq 6 \text{ dB} \\
obj_2 &= \text{BW}\,(|S_{11}|, -10 \text{ dB}) & \text{BW} \geq 4\% \\
obj_3 &= \text{AR}\,(f_0, \theta, \phi) & \text{AR} \geq 10 \text{ dB}
\end{aligned} \tag{1}
$$

(a)

(b)
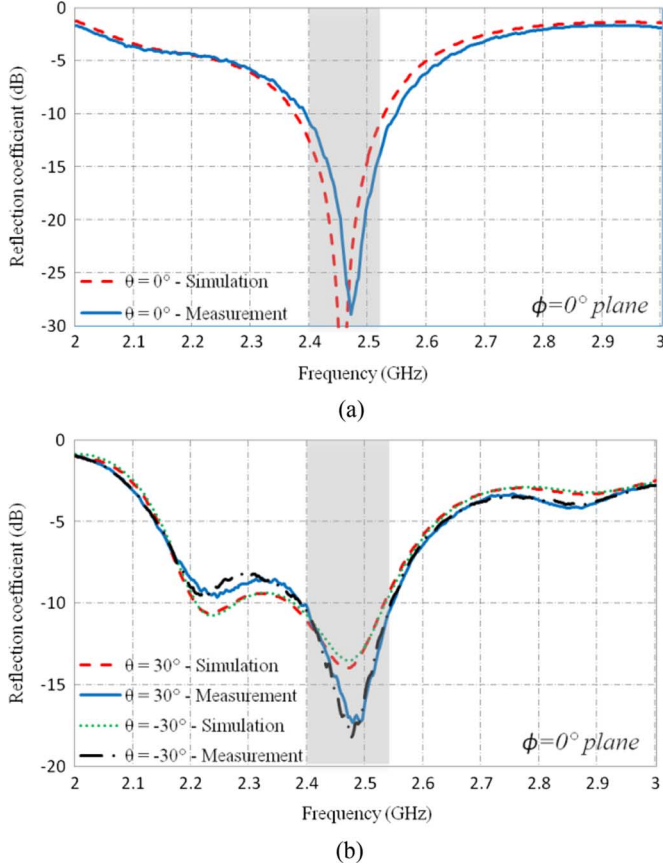
Fig. 6. Measured and simulated reflection coefficients of the MRA prototype for beam steering angles (a) $\theta = 0°$ on $\phi = 0°$ plane, (b) $\theta = 30°$ and $\theta = -30°$ on $\phi = 0°$ plane.

(a)

(b)

Fig. 7. Simulated and measured realized gain patterns of the MRA prototype for (a) $\theta = 0°$ on $\phi = 0°$ plane, (b) $\theta = 30°$ and $\theta = -30°$ on $\phi = 0°$ plane at 2.45 GHz.

where f_0 is the center frequency of the 802.11 b/g band as 2.45 GHz, θ and ϕ describe the desired beam steering direction. $|S_{11}|$ represents the magnitude of reflection coefficient, and AR is the axial ratio for polarization. These three criteria are applied simultaneously in multiobjective genetic algorithm, and in conjunction with full-wave EM analysis to find the optimized switch configurations resulting in each of the 9 beam steering directions. Note that corresponding to beam directions of ($\theta \in \{-30°, 0°, 30°\}$; $\phi \in \{0°, 45°, 90°, 135°\}$), 9 optimization problems are defined. The further details of the multiobjective algorithm are omitted here and can be found in [23].

III. ANTENNA MEASUREMENTS VS. SIMULATIONS

To validate the theoretical analysis and simulated results of the MRA, a prototype was fabricated and measured. The switch configurations for all nine desired modes are shown in Table II, where S1–S12 represent the 12 PIN diode switches used in the design as shown in Fig. 1 (0 indicates that the switch is OFF, 1 indicates that the switch is ON). The MRA prototype was designed to operate in the 802.11 b/g frequency band (2.4–2.5 GHz). The reflection coefficients and radiation patterns in terms of realized gain have been measured for all the modes. Figs. 6(a) and 6(b) show the simulated and measured reflection coefficients for the modes on $\phi = 0°$ plane with $\theta = 0°, -30°$ and $30°$. It can be seen that the common bandwidth covers IEEE 802.11 b/g frequency band. Fig. 7 shows good agreement be-
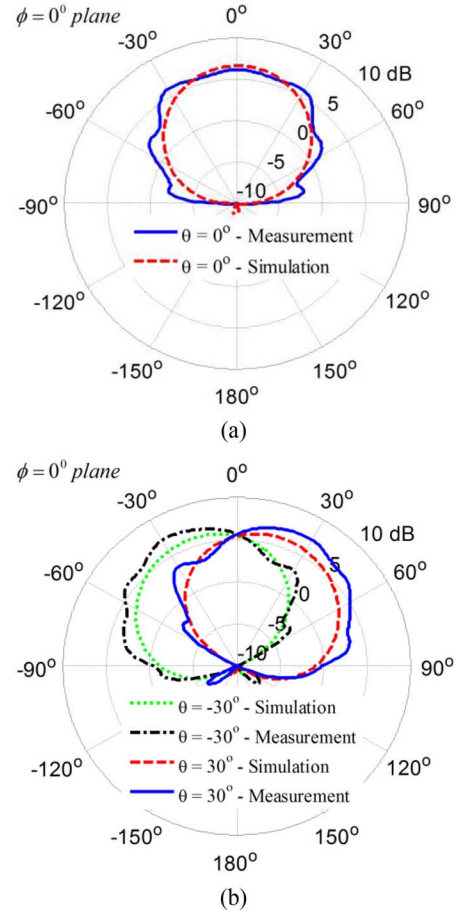
tween simulated and measured realized gain patterns for these three modes indicating that the maximum realized gain of the MRA is ~6.5 dB in each mode. Note that only copolarization components are plotted in the patterns since cross-polarization components are less than -10 dB and thus are not shown. Simulated and measured reflection coefficients and realized gain patterns for other modes on the planes ($\phi \in \{45°, 90°, 135°\}$) are shown in Figs. 8, 9, and 10, respectively. It can be seen that there is also good agreement between simulation and measurement for these modes.

IV. SYSTEM LEVEL TESTS AND CHARACTERIZATIONS

In this section, to confirm the advantages of the MRA, the system-level experimental analysis and performance characterization of MRA-based WLAN systems is presented.

A. Experimental Setup

An MRA-based WLAN system is constructed using the Universal Software Radio Peripheral (USRP) software defined radio (SDR) platform [24]. Each USRP contains a Radio Frequency (RF) transceiver and a Field Programmable Gate Array (FPGA). All USRPs are connected to a host PC through a Gigabit Ethernet connection. The baseband signal processing is performed over the host PC. The baseband signals are streamed to/from the USRPs at a rate of 25 M sample/sec. The RF
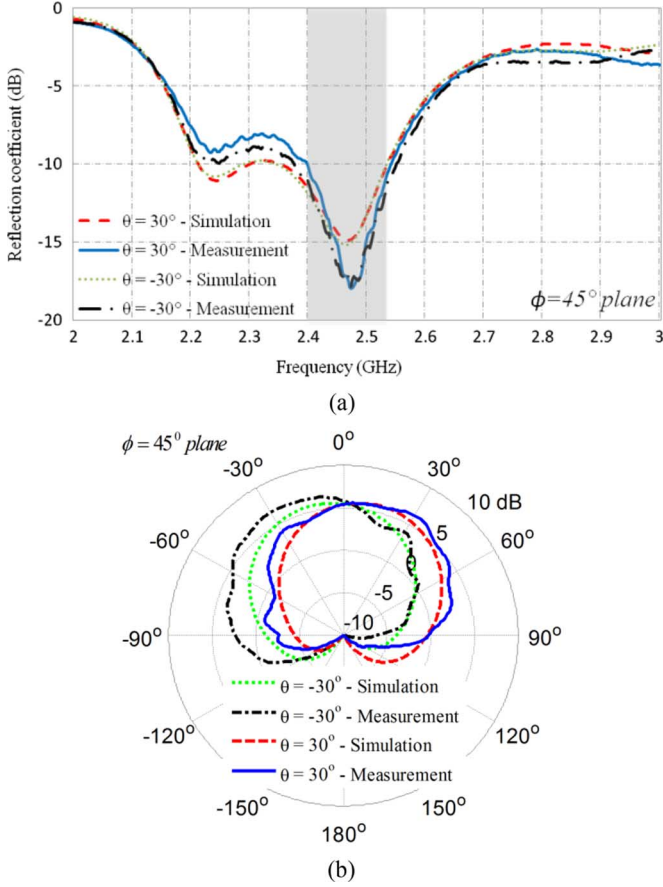
Fig. 8. Simulated and measured (a) reflection coefficients, (b) realized gain patterns of the MRA prototype for $\theta = 30°$ and $\theta = -30°$ on $\phi = 45°$ plane at 2.45 GHz.

Fig. 9. Simulated and measured (a) reflection coefficients, (b) realized gain patterns of the MRA prototype for $\theta = 30°$ and $\theta = -30°$ on $\phi = 90°$ plane at 2.45 GHz.

transceivers are then used for real time signal transmission and reception. All experiments are performed in the IEEE 802.11 b/g band at 2.5 GHz carrier frequency with a 10 MHz signal bandwidth.

As shown in Fig. 11, the system consists of two nodes (node A and node B) communicating to each other. Each node is equipped with one antenna. In this work, one of the two nodes is equipped with an omni-directional antenna, while the other node is equipped with a MRA (node A is equipped with omni-directional antenna, while node B is equipped with MRA). The MRA antenna has a total of nine different radiation patterns $(\theta \in \{-30°, 0°, 30°\}; \phi \in \{0°, 45°, 90°, 135°\})$. The pattern selection is performed through a 12-line digital control cable driven from an FPGA on a Zedboard [25]. The timing of all USRPs and the FPGA that drives the antenna switches are aligned with one reference Pulse Per Second (PPS) signal. Another system architecture where both nodes are equipped with omni-directional antennas is used for comparison purposes.

B. Experimental Framework

Fig. 12 shows the transmission frame structure used for performance characterization. The transmission frame consists of two main intervals: 1) training interval, and 2) data transmission interval. The training interval consists of 9 training segments used for MRA pattern train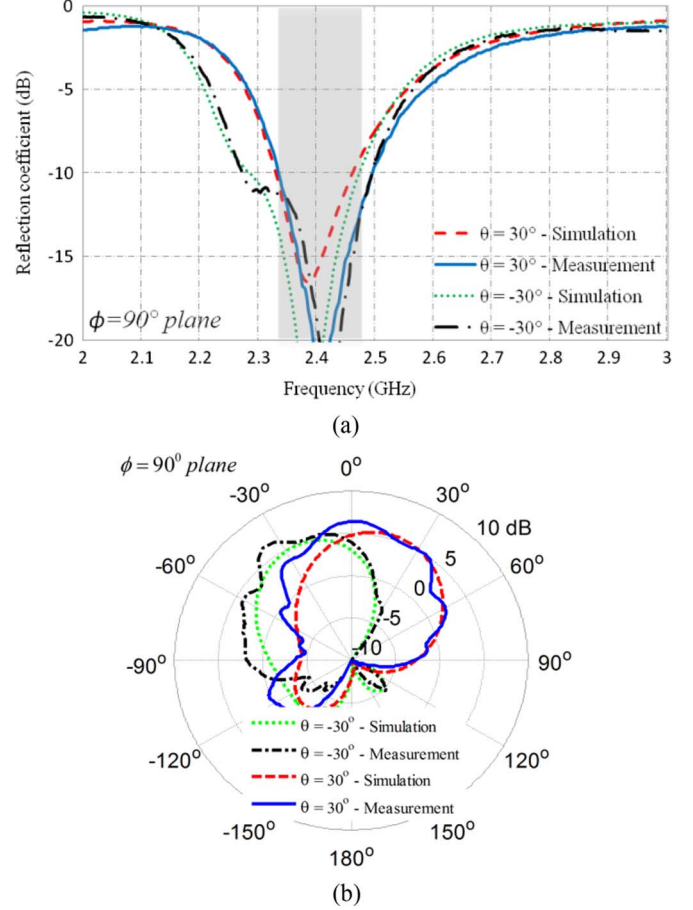ing. The MRA radiation pattern is changed at the segment edge such that, each training segment corresponds to one of the 9 MRA radiation patterns. At the end of the training interval, the received signal power for each pattern is calculated, and the pattern that maximizes the received signal power is selected.

During the data transmission interval, useful data transmission takes place. The data transmission interval consists of several data frames that have the same frame structure as in the IEEE 802.11g systems [26]. Each data frame consists of 125 Orthogonal Frequency Division Multiplexing (OFDM) symbols with 64 subcarriers per OFDM symbol.

C. Experimental Environment

The experimental analysis is conducted in the Wireless Systems and Circuits Laboratory (WSCL) within Engineering Hall at the University of California, Irvine. Fig. 13 shows a floor plan for the area where the experiments are performed, and present a typical laboratory environment with measurement workstations, tables, metallic surfaces, etc. The outer walls of the building are either concrete walls or glass walls with steel pillars, while the inner walls are dry walls with steel pillars.

To enrich the experimental analysis, the two communicating nodes are placed at different positions inside and outside the laboratory to create a variety of Line Of Sight (LOS) and non-LOS
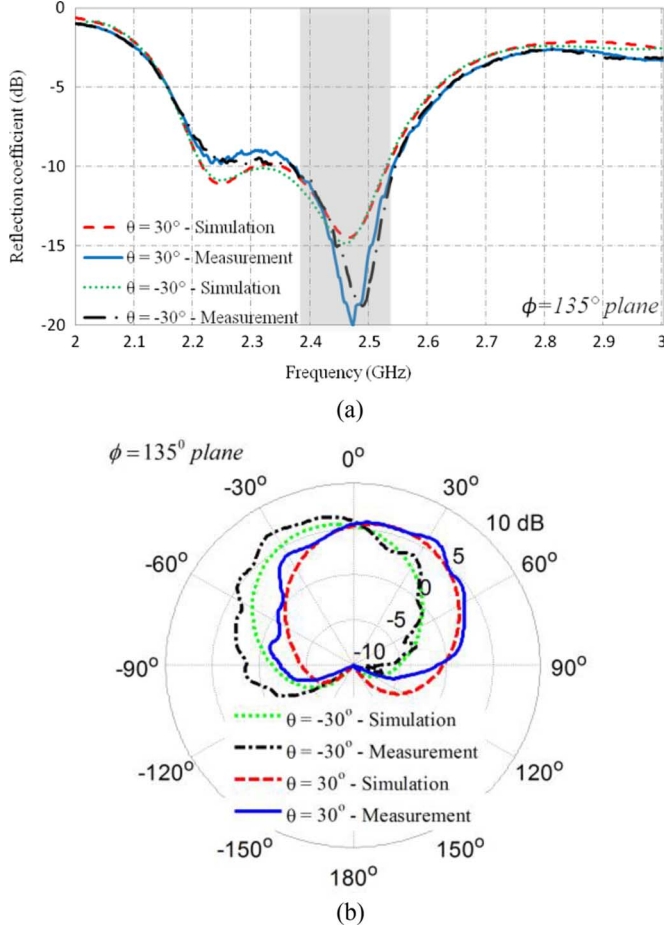
(a)

(b)

Fig. 10. Simulated and measured (a) reflection coefficients, (b) realized gain patterns of the MRA prototype for $\theta = 30°$ and $\theta = -30°$ on $\phi = 135°$ plane at 2.45 GHz.

TABLE II
SWITCH CONFIGURATIONS FOR NINE MODES OF OPERATION

θ	ϕ	S1	S2	S3	S4	S5	S6	S7	S8	S9	S10	S11	S12
0°	0°	0	0	0	0	0	0	0	0	0	0	0	0
30°	0°	0	1	1	0	0	1	0	1	0	0	0	1
-30°	0°	1	0	0	0	1	0	1	0	0	1	1	0
30°	45°	1	0	1	0	0	1	0	1	0	0	0	1
-30°	45°	1	0	0	0	1	1	0	0	0	0	1	0
30°	90°	1	0	0	1	0	0	1	0	0	0	1	1
-30°	90°	0	1	1	0	0	0	1	1	1	0	1	1
30°	135°	0	1	0	0	1	0	1	0	0	1	1	0
-30°	135°	0	1	1	0	0	1	0	1	0	0	1	0

environments (the different circle and square dots are the different positions that node B and node A are placed in during the experiments). In addition, different MRA orientations are tested such that the two communicating nodes are facing each other, opposite to each other, or side to side (the black arrows going out from node B represent different directions where the MRA antenna is pointing at during the experiments).

D. Experimental Results

In this analysis, the performance of the MRA-based IEEE 802.11g system is evaluated and compared to that of the legacy
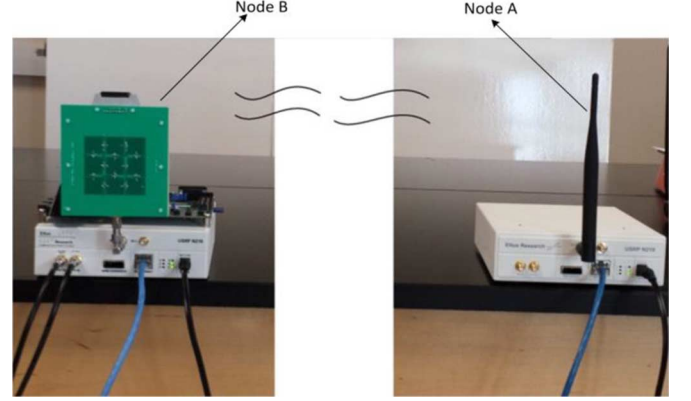

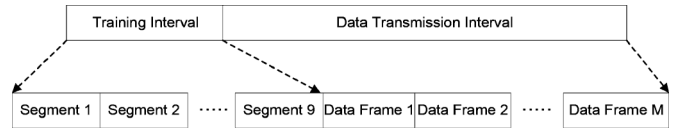Fig. 11. MRA-based wireless system using USRP platforms.

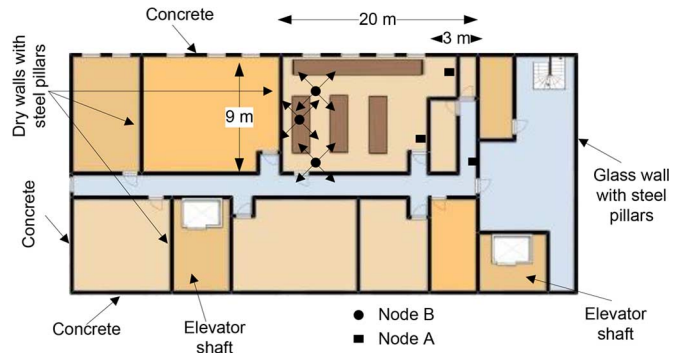Fig. 12. Transmission frame structure.

Fig. 13. Floor plan for the area where the experiments are conducted.

omni-directional antenna based system. For comparison purposes, three different performance metrics are used: 1) The effective SNR, 2) the achievable rate, and 3) the average un-coded Bit Error Rate (BER). The SNR is defined as the ratio between the received signal power and the total system noise power. One way to calculate the effective SNR in experimental analysis is by calculating the Error Vector Magnitude (EVM) defined as the distance between the received symbols after equalization and the original transmitted symbols. Using the EVM to SNR conversion method in [27], the SNR is calculated as $\text{SNR} = 1/\overline{\text{EVM}}^2$, where $\overline{\text{EVM}}$ is the average EVM. The achievable rate is defined as the maximum data rate that the wireless system could achieve at certain SNR. The average achievable rate is calculated in terms of the SNR as:

$$R = \frac{1}{N.M} \sum_{n=1}^{N} \sum_{m=1}^{M} \log_2 \left(1 + \text{SNR}_{n,m}\right), \quad (2)$$

where N, M are the total number of data frames and OFDM symbols per frame respectively.

First, we characterize the performance gain achieved using MRA in different experimental environments. Fig. 14 shows
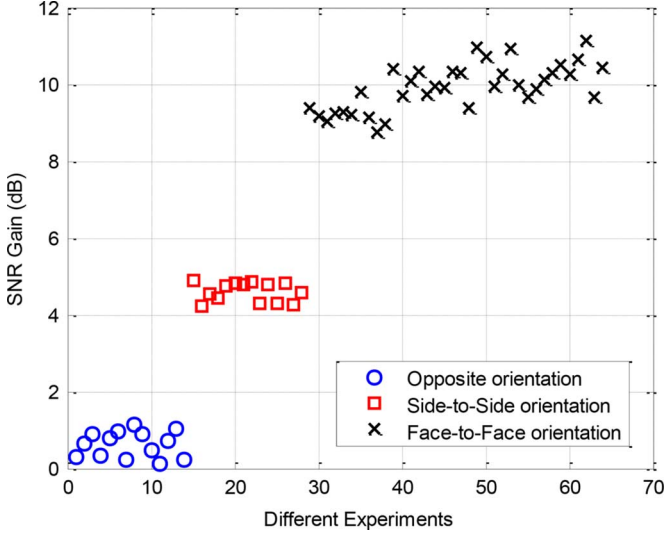
Fig. 14. SNR gain for MRA-based system compared to omni-directional antenna based system at different antenna orientations, with 0 dBm transmit power.
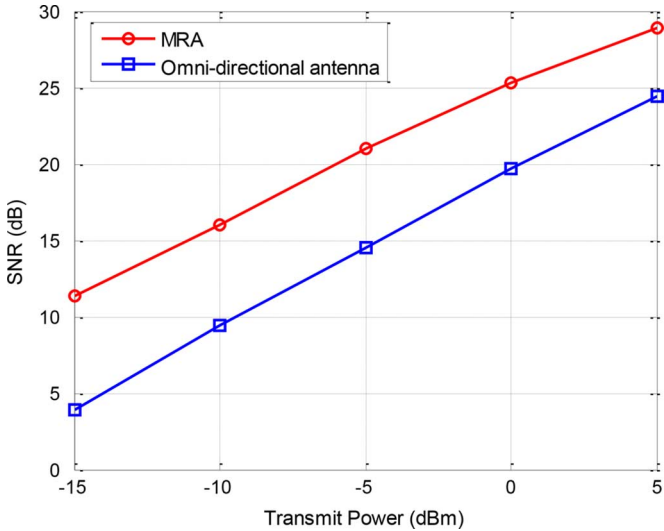

Fig. 16. Achievable rate for MRA-based and omni-directional antenna based systems at different transmit power values.

Fig. 15. Effective SNR for MRA-based and omni-directional antenna based systems at different transmit power values.

Fig. 17. BER for MRA-based and omni-directional antenna based systems at different transmit power values with different modulation schemes.

the SNR gain achieved using MRA compared to the omni-directional antenna at different antenna orientations. The results show that the worst SNR gain is achieved when the back of the MRA antenna is facing the other node. In this scenario, a significant part of the signal power is received through the MRA back-loops. Although the opposite orientation has the worst performance, the MRA antenna still achieves better performance than the omni-directional antenna ($\sim$1 dB better SNR), mainly due to the signal reflections. On the other hand, the face-to-face orientation shows the best performance, where the MRA could achieve $\sim$10 dB better performance than omni-directional antenna. The reason is that in face-to-face orientation, most of the signal power is received through the main loops of the MRA. The side-to-side orientation is in the middle between other orientations.

In typical scenarios, the system will be exposed to all different orientations over time. Accordingly, calculating the av-
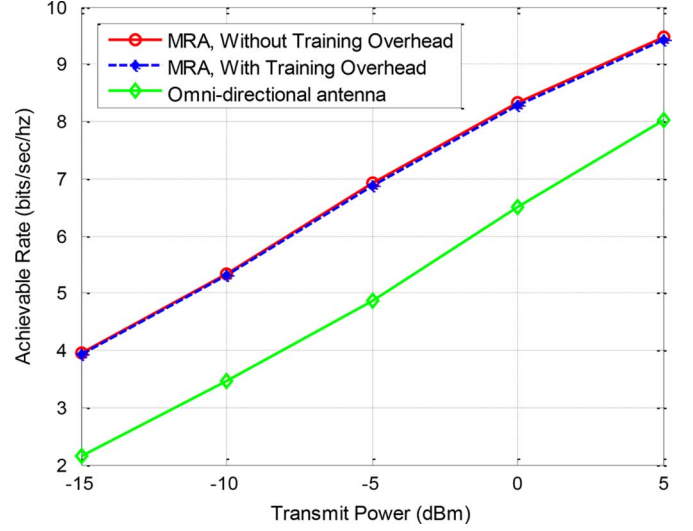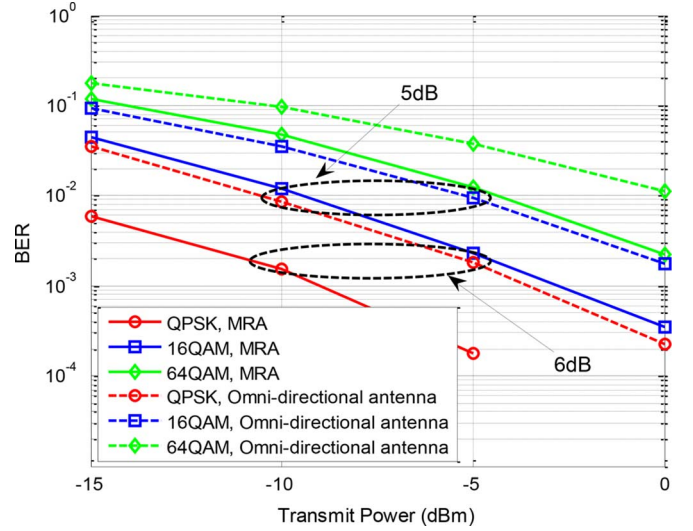
erage performance gives an indication of how MRA performs compared to omni-directional antenna on the average sense. In the following analysis, the performance is averaged over several experiments with different orientations and node positions. Fig. 15 shows the effective SNR for MRA-based and omni-directional antenna based systems at different transmit power values. The results show that, using MRA achieves an average of 5–6 dB SNR gain compared to the legacy omni-directional antenna systems.

Unlike omni-directional antenna systems, MRA-based systems require pattern training, which negatively impacts the overall system capacity. Therefore, for fair comparison, the MRA training overhead should be considered. In this analysis, the achievable rate of both MRA-based and omni-directional antenna based systems is evaluated. The MRA training overhead is set to $\sim$0.5% (i.e., MRA training interval/data transmission interval $=0.005$). Fig. 16 shows the achievable rate at different transmit power values when MRA training

overhead is considered. The results show that, even after training overhead is considered, MRA-based systems could achieve ~2 bits/sec/hz more data rate compared to legacy omni-directional antenna systems.

The overall performance is also characterized for different modulation schemes. Fig. 17 shows the average BER for both MRA-based and omni-directional antenna based systems. The results show that using MRA achieves $\sim 5 - 6$ dB SNR gain compared to omni-directional antenna based systems, which confirms the results shown in Fig. 15.

V. CONCLUSION

This paper presented a full model of a multifunctional reconfigurable antenna (MRA) with the main goal of enhancing the spectral efficiency of existing and future wireless networks. The presented MRA is capable of steering its main beam in nine directions ($\theta \in \{-30°, 0°, 30°\}; \phi \in \{0°, 45°, 90°, 135°\}$) by reconfiguring the geometry of the parasitic pixel surface. This surface consists of a grid of 3×3 electrically small square-shaped metallic pixels, and the geometry of this surface is altered by switching ON/OFF the interconnecting PIN diode switches placed between adjacent metallic pixels. To validate the theoretical analyses and simulations, a prototype of MRA operating in the IEEE 802.11 b/g frequency band has been fabricated and measured. The good agreement between measured and simulated results confirmed the accuracy of the theoretical results. The average realized gain values of the MRA prototype are ~6.5 dB in all modes of operation over the 2.4–2.5 GHz frequency band. The MRA was also implemented in a practical system setting, where the system level experimental performance of an MRA equipped WLAN platform was tested and characterized in typical indoor environments. The results showed that the MRA equipped WLAN systems could achieve an average of 6 dB Signal to Noise Ratio (SNR) gain compared to legacy omni-directional antenna equipped systems with minimal training overhead.

ACKNOWLEDGMENT

REFERENCES

[1] L. N. Pringle *et al.*, "A reconfigurable aperture antenna based on switched links between electrically small metallic patches," *IEEE Trans. Antennas Propag.*, vol. 52, no. 6, pp. 1434–1445, June 2005.

[2] J. T. Bernhard, "Reconfigurable antennas," in *Synthesis Lectures on Antennas*. San Rafael, CA, USA: Morgan & Claypool, 2007.

[3] "Special issue on multifunction antennas and antenna systems," *IEEE Trans. Antennas Propag.*, vol. 54, no. 2, Feb. 2006.

[4] B. A. Cetiner, H. Jafarkhani, J.-Y. Qian, H. J. Yoo, A. Grau, and F. De Flaviis, "Multifunctional reconfigurable MEMS integrated antennas for adaptive MIMO systems," *IEEE Commun. Mag.*, vol. 42, no. 12, pp. 62–70, Dec. 2004.

[5] B. Akbar, M. Sayeed, and V. Raghavan, "Maximizing MIMO capacity in sparse multipath with reconfigurable antenna arrays," *IEEE J. Sel. Topics Signal Process.*, vol. 1, no. 1, pp. 156–166, June 2007.

[6] B. A. Cetiner, E. Sengul, E. Akay, and E. Ayanoglu, "A MIMO system with multifunctional reconfigurable antennas," *IEEE Antennas Wireless Propag. Lett.*, vol. 5, no. 1, pp. 463–466, Dec. 2006.

[7] D. Piazza *et al.*, "Design and evaluation of a reconfigurable antenna array for MIMO systems," *IEEE Trans. Antennas Propag.*, vol. 56, no. 3, pp. 869–881, Mar. 2008.

[8] D. Piazza *et al.*, "Performance improvement of a wideband MIMO system by using two-port RLWA," *IEEE Antennas Wireless Propag. Lett.*, vol. 8, pp. 830–834, 2009.

[9] P. Mookiah, D. Piazza, and K. R. Dandekar, "Reconfigurable spiral antenna array for pattern diversity in wideband MIMO communication systems," in *Proc. IEEE Antennas Propag. Soc. Int. Symp.*, July 2008, pp. 1–4.

[10] H. K. Pan *et al.*, "Increasing channel capacity on MIMO system employing adaptive pattern/polarization reconfigurable antenna," in *Proc. IEEE Antennas Propag. Soc. Int. Symp.*, June 2007, pp. 481–484.

[11] J. D. Boerman and J. T. Berhard, "Performance study of pattern reconfigurable antennas in MIMO communication systems," *IEEE Trans. Antennas Propag.*, vol. 56, no. 1, pp. 231–236, Jan. 2008.

[12] ANSOFT HFSS, Version 11.0, Build July 18, 2007 [Online]. Available: http://www.ansys.com, ANSYS Corporation [Online]. Available:

[13] Y. Kuwahara, "Multiobjective optimization design of Yagi-Uda antenna," *IEEE Trans. Antennas Propag.*, vol. 53, no. 6, pp. 1984–1992, June 2005.

[14] C. M. D. J. Van Coevorden, S. G. Garcia, M. F. Pantoja, A. R. Bretones, and R. G. Martin, "Microstrip-patch array design using a multiobjective GA," *IEEE Antennas Wireless Propag. Lett.*, vol. 4, pp. 100–103, 2005.

[15] D. W. Boeringer and D. H. Werner, "Beźier representations for the multiobjective optimization of conformal array amplitude weights," *IEEE Trans. Antennas Propag.*, vol. 54, no. 7, pp. 1964–1970, July 2006.

[16] J. S. Petko and D. H. Werner, "The pareto optimization of ultrawideband polyfractal arrays," *IEEE Trans. Antennas Propag.*, vol. 56, no. 1, pp. 97–107, Jan. 2008.

[17] Z. Li, D. Rodrigo, L. Jofre, and B. Cetiner, "A new class of antenna array with a reconfigurable element factor," *IEEE Trans. Antennas Propag.*, vol. 61, no. 4, pp. 1947–1955, Apr. 2013.

[18] Rogers Corp., Microwave Products Tech. Information 2012, One Technology Drive, CT 06263.

[19] SMP 1345 Series, Skyworks Corporation [Online]. Available: [Online]. Available: http://www.skyworksinc.com

[20] HP 0603, Chip Inductor Series, Coilcraft Corporation [Online]. Available: http://www.coilcraft.com [Online]. Available:

[21] GQM 0603, SMD Capacitor Series, Murata Corporation [Online]. Available: http://www.murata.com [Online]. Available:

[22] R. F. Harrington, "Reactively controlled directive arrays," *IEEE Trans. Antennas Propag.*, vol. 26, no. 3, pp. 390–395, May 1978.

[23] X. Yuan, Z. Li, D. Rodrigo, H. S. Mopidevi, O. Kaynar, and B. A. Cetiner, "A parasitic layer-based reconfigurable antenna design by multi-objective optimization," *IEEE Trans. Antennas Propag.*, vol. 60, no. 6, pp. 2690–2701, June 2012.

[24] Universal Software Radio Peripheral (USRP) Datasheet [Online]. Available: https://www.ettus.com/product/category/USRP-Networked-Series

[25] The ZedBoard [Online]. Available: http://www.zedboard.org

[26] IEEE Standard for Information Technology-Telecommunications and Information Exchange Between Systems Local and Metropolitan Area Networks-Specific Requirements Part 11: Wireless LAN Medium Access Control (MAC) and Physical Layer (PHY) Specifications Mar. 2012, IEEE Std 802.11-2012 (Revision of IEEE Std 802.11-2007).

[27] H. Arslan and H. Mahmoud, "Error vector magnitude to SNR conversion for nondata-aided receivers," *IEEE Trans. Wireless Commun.*, vol. 8, no. 5, pp. 2694–2704, May 2009.
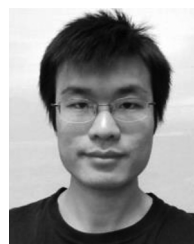
Zhouyuan Li received the M.S. degree from Shanghai University, Shanghai, China, in 2010 and the Ph.D. degree from Utah State University, Logan, UT, USA, in 2014.

His research interests include multi-funtional reconfigurable antenna, antenna array, and microwave circuit.

Elsayed Ahmed received the B.Sc. and M.Sc. degrees from the Electronics and Communications Department, Cairo University, Egypt in 2006 and 2010, respectively, and the Ph.D. degree from the University of California, Irvine, CA, USA, in 2014.

He worked as a Senior System Design Engineer at Newport Media Inc. from 2006 to 2010. His research interest includes full-duplex wireless communications, digital signal processing, and algorithm design for wireless communication systems.

Ahmed M. Eltawil (S'97–M'03–SM'14) received the M.Sc. and B.Sc. degrees (with Hons.) from Cairo University, Giza, Egypt, in 1999 and 1997, respectively, and the Ph.D. degree from the University of California, Los Angeles, USA, in 2003.

He is an Associate Professor at the University of California, Irvine, CA, USA. He is the founder and director of the Wireless Systems and Circuits Laboratory. His current research interests are in low power digital circuit and signal processing architectures for wireless communication systems.

Dr. Eltawil has been on the technical program committees and steering committees for numerous workshops, symposia and conferences in the area of VLSI, and communication system design. He received several distinguished awards, including the NSF CAREER award in 2010 supporting his research in low power wireless systems.

Bedri A. Cetiner (M'99) received the Ph.D. degree in electronics and communications engineering from the Yildiz Technical University, Istanbul, in 1999.

He is an Associate Professor in the Department of Electrical Engineering, Utah State University, Logan, UT, USA. From November 1999 to June 2000, he was with the University of California, Los Angeles, as a NATO Science Fellow. He then joined the Department of Electrical Engineering and Computer Science, University of California, Irvine, where he worked as a Research Specialist from June 2000 to June 2004. From July 2004 until July of 2007, he worked as an Assistant Professor in the Department of Space Science and Engineering, Morehead State University, Kentucky. In August 2007, he joined Utah State University, Logan. His research focuses on the applications of micro-nano technologies to a new class of micro-/millimeter-wave circuits and systems, and intelligent wireless communications systems with an emphasis on the multifunctional reconfigurable antennas (MRA) for use in cognitive multi-input multi-output (MIMO) systems. He is the Principal Inventor of six technologies including microwave laminate compatible RF MEMS technology and MRA equipped MIMO systems.

Prof. Cetiner is a member of the IEEE Antennas and Propagation, Microwave Theory and Techniques, and Communication societies.